Assessing the Contribution of Active and Passive Stresses in *C. elegans* Elongation

Martine Ben Amar,[1,2,*] Paul Qiuyang-Qu,[1] Thanh Thi Kim Vuong-Brender,[3] and Michel Labouesse[4]
[1]*Laboratoire de Physique Statistique, Ecole Normale Supérieure, PSL Research University; Sorbonne Université, UPMC Univ Paris 06; CNRS; 24 rue Lhomond, 75005 Paris, France*
[2]*Institut Universitaire de Cancérologie, Faculté de médecine, Université Pierre et Marie Curie-Paris 6, 91 Bd de l'Hôpital, 75013 Paris, France*
[3]*MRC Laboratory of Molecular Biology, Francis Crick Avenue, Cambridge Biomedical Campus, Cambridge CB2 0QH, United Kingdom*
[4]*Laboratoire de Biologie du Développement—Institut de Biologie Paris Seine (LBD—IBPS), Sorbonne Université, UPMC Univ Paris 06, CNRS, Paris, France*

(Received 1 August 2018; revised manuscript received 17 October 2018; published 28 December 2018)

The role of the actomyosin network is investigated in the elongation of *C. elegans* during embryonic morphogenesis. We present a model of active elongating matter that combines prestress and passive stress in nonlinear elasticity. Using this model we revisit recently published data from laser ablation experiments to account for why cells under contraction can lead to an opening fracture. By taking into account the specific embryo geometry, we obtain quantitative predictions for the contractile forces exerted by the molecular motors myosin II for an elongation up to 70% of the initial length. This study demonstrates the importance of active processes in embryonic morphogenesis and the interplay between geometry and nonlinear mechanics during morphological events. In particular, it outlines the role of each connected layer of the epidermis compressed by an apical extracellular matrix that distributes the stresses during elongation.

DOI: 10.1103/PhysRevLett.121.268102

Mechanical stresses play a crucial role in animal embryo genesis. At the macroscopic level, differential growth generates compressive stresses creating the circumvolutions of intestine [1–3], brain cortex [4–6], and fingerprints of skin [7,8]. The folding of tissues is then directly linked to the coupling between volumetric growth, tissue properties, and geometry. At the cellular level, the interplay between mechanics and morphological events such as division, migration, and tissue organization is much more subtle. The high deformability of cells is counterbalanced by the cellular filament networks, especially by the actomyosin cortex. It comprises a network of cross-linked actin filaments located below the plasma membrane, so that the local cell contractility results from the myosin molecular motors which transform the chemical energy of ATP hydrolysis into contractile stresses. How these microscopic processes at the cell level cooperate to induce shape transition at the tissue level is central in "active matter." At early stages in small organisms such as *Drosophila* [9] or *C. elegans* [10], the number of cells is relatively small and the structure is simple enough, giving perhaps a way to bridge scales between microscopic activity and observable tissue displacements. Both of these biological species are considered as model systems where the theoretical framework of active matter [11–15] can be applied and more importantly quantified by analyzing experimental data. Here we investigate the early stage of *C. elegans* elongation up to 70% when the embryo contains 65 epidermal cells in the cortical position in an ovoid shell. Among available approaches, laser cuts in different locations on live embryos allow us to evaluate either the tension or the stiffness [16], quantities necessary to assess the active stresses at the origin of the elongation [17,18]. Since, in this process, there is no cytokinesis or apoptosis and no position exchange between neighboring cells, we select a continuum approach of active matter to predict the fracture opening. However, as highlighted in Refs. [19,20], the difficulty in active matter consists in evaluating the stresses: active or passive for samples with complex geometry and elastic properties. To this end, one must comprehend the nonlinearities of shape transformations in these small organisms with a limited information on mechanical quantities.

The aim of this Letter is to investigate this problematics when only some characteristics are known for *C. elegans* embryos. Our scope is to estimate the activity of the molecular motors and to compare it to the elastic resistance. For that, we establish an analytical model based on nonlinear elasticity for soft tissues and compare our predictions with measurements by laser ablation [16]. The proposed treatment can be adapted to other morphogenetic events in embryogenesis.

Laser ablation.—Fracture opening gives a way to determine the forces at the cellular level. This technique helps to experimentally deduce the tensile stress in the perpendicular direction to the fracture line when the cell stiffness is known. Conversely, when the stresses are well

 © 2018 American Physical Society

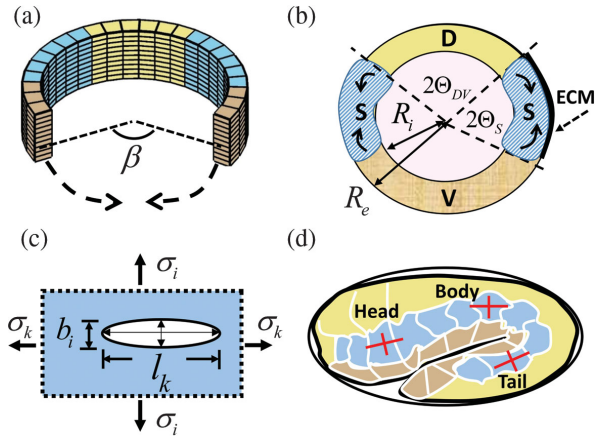

FIG. 1. The ventral enclosure of *C. elegans*. (a) Schematic representation before enclosure. (b) Horizontal section at enclosure. Different colors are chosen: yellow for the dorsal (D), blue for the seam (S), and brown for the ventral (V) cells. (c) Schema of a planar fracture under tensile stresses. (d) Position of laser fractures achieved in the embryo [16].

identified, it gives some insights on the fiber network organization. Indeed, the crack opening in linear elasticity is an ellipse [21] and the shape factor (opening b_i along x_i divided by the crack length l_k along x_k) is given by $\mathcal{F}_{ik} = b_i/l_k \sim 2\sigma_i/E$, where σ_i is the tension and E the Young modulus, see Fig. 1(c). For $\mathcal{F}_{ik}$, other stress components than σ_i do not play a role and for an anisotropic sample, E must be replaced by E_i the stiffness in the x_i direction [16].

In a recent work [16], Vuong-Brender *et al.* apply this technique in different parts of *C. elegans* [in Fig. 1(d)] and demonstrate that the cracks always open both in the dorsoventral (DV) and in the anterior-posterior (AP) directions. If the crack opening is not a surprise in AP, it is more puzzling in the DV direction for various reasons, Fig. 1(d). First, cracks cannot open in compression (except in some very specific conditions [22]). Because of volume conservation, an extension in AP leads automatically to a contraction in DV. In addition, myosin II, the actin molecular motors have been observed [23–26] in the seam (S) domain [blue in Figs. 1(a),1(b),1(d)], and these motors are contractile. Even more intriguing, in S cells, the opening is larger in the DV than in the AP direction [16]. The theoretical interpretation of these experiments cannot be captured by the linear elasticity framework. To recover the shape factor $\mathcal{F}_{ik}$ requires evaluating first the state of stresses or strains inside the embryo before elongation and then incorporating the active stresses due to molecular motors. By coupling them, the modeling must recover the results of the laser ablation but also the possibility to elongate the embryo up to 70%. Nonetheless, in nonlinear elasticity, and to the best of our knowledge, there is no general formula for crack opening but only local analysis of the stresses at both ends [27,28]. A simple analogy between linear and nonlinear elasticities suggests to replace σ by the equivalent Cauchy stress σ_i and E by the local stiffness E_i. The following addresses the evaluation of these two quantities in the nonlinear elasticity framework beginning first by the geometry analysis.

Geometry and strains.—The morphogenetic events of the embryo elongation consist of cell intercalation and ventral enclosure [10]. The displacements of matter are strongly constrained by the limited space and induce significant strains [29]. In particular, the ventral enclosure, schematized by Fig. 1(a), cannot be achieved without local forces to join the two parts of the epithelial cortex, as demonstrated by myosin accumulation [23,24]. Hence, when elongation begins, the tissues have already stored prestrains and prestresses [20] and the measurements in Ref. [16] result from those cumulated stresses. Their evaluation requires a complete knowledge of the history, which is difficult to assess. A possible simplified scenario will be the enclosure of a cylindrical partial shell with a lacking angular sector β, see Fig. 1(a), by orthoradial stretching. But this shell is made of a nonhomogeneous epidermis with 3 kinds of cells called hereafter dorsal (D), seam (S), and ventral (V) cells; see Fig. 1(b). Once the suture is achieved, the embryo becomes a composite cylinder made of a row of epithelial cells and nascent intestine. Besides, it is covered by the extracellular matrix (ECM), a thin layer of secreted proteins. In the stress-free configuration, before enclosure, the D cells occupy one sector between $[-\phi_{DV}, \phi_{DV}]$, S cells are located between $[\phi_{DV}, \tilde{\beta} - \phi_{DV}]$, and V cells fill the remaining sector up to $\tilde{\beta} = \pi - \beta/2$ [Fig. 1(a) and in the Supplemental Material [30]]. From the mechanical viewpoint, we do not make a distinction between the D and V cells and now call them DV cells. As shown in the Supplemental Material [30], at full enclosure [**FE**, Fig. 1(b)], the position of material points are defined by R, Θ, Z and then becomes r, θ, z with elongation. At **FE**, the epidermis lies between the inner R_i and the outer R_e radius. It is possible to map the stress-free configuration onto the current one and then to define the elastic strains, but one must keep in mind that the experimental results refer to the beginning of elongation which is not a stress-free state. This distinction is essential in nonlinear elasticity. We call G the angular stretch defined by $\theta = G\Theta_i$, which varies with the axial stretch Λ_Z and the domain area. We hypothesize that at **FE**, all parts are stretched in the orthoradial direction so $G_0 > 1$. The two unknown parameters of the initial geometry (e.g., $\tilde{\beta}$ and Θ_{DV}) are determined in the Supplemental Material [30] by arclength measurements [16]. Looking for the simplest solution where strains and stresses remain diagonal, the deformation gradient tensor defined by $\mathbf{F} = \mathrm{Diag}(\Lambda_R, \Lambda, \Lambda_Z)$ is then $\mathbf{F} = \mathrm{Diag}(\partial r/\partial R, Gr/R, dz/dZ)$. Resulting from both enclosure and elongation, the elastic tensor $\mathbf{F_e}$ defined by Diag $(\lambda_R, \lambda, \lambda_Z)$ reads $\mathbf{F_e} = \mathbf{F}\mathbf{F_0}$. $\mathbf{F_0}$ is the prestretch tensor defined by 2 independent eigenvalues:

$\mathbf{F_0} = \mathrm{Diag}((\lambda_0\lambda_{0Z})^{-1}, \lambda_0, \lambda_{0Z})$, since the incompressibility imposes $\lambda_R = 1/(\lambda\lambda_Z)$. (See also the Supplemental Material [30]). These tensors are defined everywhere in the cylinder and are different in S or DV domains. Only the elongations Λ_Z and λ_{0Z} will remain identical in all parts for reasons of integrity. Since there is no cell division during the process, the volume conservation in the epithelium gives

$$r^2 - r_i^2 = \frac{1}{G\Lambda_Z}(R^2 - R_i^2), \tag{1}$$

which allows us to calculate G, knowing that at the border of the interior zone, $\Lambda = r_i/R_i = 1/\sqrt{\Lambda_Z}$. In the Supplemental Material [30], it is shown how the angular stretch G for S and DV cells, Fig. 2, is obtained from measurements of the circumferential lengths published in Ref. [16]. Since data are available only at $\Lambda_Z = 1.3, 1.5$, extrapolation at $\Lambda_Z = 1$ is used. Agreement between modeling and experimental data [30] validates the first steps with an epithelium thickness of order 2 μm. Mechanical stresses can now be evaluated.

Equilibrium equations and boundary conditions.—The crack opening reaches its finite value after only a few seconds, which is in the same order of magnitude as the velocities of actomyosin flows (in the order of 1 μm/s [31,32]). Focusing on the equilibrium value of the slit opening, we can neglect viscoelasticity [33,34]. Then, in cylindrical geometry, the Cauchy stress σ, diagonal as the deformation gradient tensor $\mathbf{F_e}$, satisfies

$$\frac{\partial\sigma_r}{\partial r} + \frac{1}{r}(\sigma_r - \sigma_\theta) = 0, \tag{2}$$

where σ_r and σ_θ are the radial and orthoradial components in the current configuration. This equation is identical in linear elasticity [35]. Equation (2) requires only one boundary condition, chosen at the apical border, just below the ECM whose thickness is about 10^{-2} the embryo radius [16,26]. So, it imposes a weak compressive surface stress, $\sigma_r \sim 0$, during elongation. Defining W_P as the passive elastic energy density, each stress component becomes $\sigma_k = \lambda_k(\partial W_P/\partial\lambda_k) + \sigma_k^a - p$ [17,18], where p is a Lagrange parameter ensuring the incompressibility and σ_k^a the active stress which only exists in the S cells. σ_k^a can be decomposed into a volumetric $\boldsymbol{\sigma}^{a,v}$ and a deviatoric $\boldsymbol{\sigma}^{a,d}$ part defined by: $\boldsymbol{\sigma}^{a,v} = \zeta_{a,v}\mathbf{I}$ and $\boldsymbol{\sigma}^{a,d} = \zeta\mathrm{Diag}(0,1,-1)$ [14,19]. $\zeta_{a,v}$ may be included into the Lagrange parameter p (a detailed demonstration can be found in the Supplemental Material [30]). Conversely, the deviatoric part is a traceless tensor with no specific sign. Finally, the definition of a new energy functional [36]: $\tilde{W}_P = W_P[(\lambda\lambda_Z)^{-1}, \lambda, \lambda_Z]$ enforces automatically incompressibility giving:

$$\sigma_\theta = \sigma_\theta^p + \sigma_r + \zeta; \qquad \sigma_z = \sigma_Z^p + \sigma_r - \zeta;$$
$$\sigma_\theta^p = \lambda\frac{\partial\tilde{W}_P}{\partial\lambda}; \qquad \sigma_Z^p = \lambda_Z\frac{\partial\tilde{W}_P}{\partial\lambda_Z}, \tag{3}$$

where σ_θ^p and σ_Z^p decouple from the active part ζ. Once Eq. (2) is solved, all stresses can be calculated explicitly [30]. Since fractures are made superficially on the outer surface where $\sigma_r \sim 0$, only σ_θ and σ_z are the components of interest for our study.

Evaluation of the stresses and fracture opening.—In these epithelial cells, it was found [25] that both microtubules and actin filaments are oriented mainly in the orthoradial direction in both cells. So we choose the simplest constitutive law as a superposition of a matrix and a fiber network elasticity:

$$W_P = \frac{\mu}{2}(\lambda_R^2 + \lambda^2 + \lambda_Z^2 - 3) + \frac{\tau}{4}(\lambda^2 - 1)^2, \tag{4}$$

when orientation along θ is imposed. Such superposition is currently achieved with some variants concerning the last term [37,38]. Choosing the S cell coefficient μ_S as the unit of elastic energy, we estimate that $\mu_{DV} > 1$ to represent a stiffer material and $\tau_S < \tau_{DV}$, to represent a weaker degree of fiber alignment in S cells. Since orientation is the same for actin or microtubules [16,25], a unique coefficient τ involves both filaments.

At **FE**, the state of the cylinder is characterized by 3 independent prestrain quantities which are the orthoradial stretches (λ_{0S} and λ_{0DV}) and the axial stretch λ_{0Z}; see the Supplemental Material [30]. Within the thin epithelium approximation, $\eta = 1 - R_i^2/R^2 \ll 1$, one easily finds $G_0 \sim \lambda_0\sqrt{\lambda_{0Z}}$, from Eq. (1). From the geometry, the lacking angle of the sector reads $\beta \sim 2(\pi - \tilde{\beta}) \sim 2\pi[1 - (\sqrt{\lambda_{0Z}}\lambda_{0S})^{-1}]$. In addition, λ_{0S} and λ_{0DV} values must be compatible with the continuity of the orthoradial stresses $\sigma_{\theta,S} = \sigma_{\theta,DV}$ at **FE**,

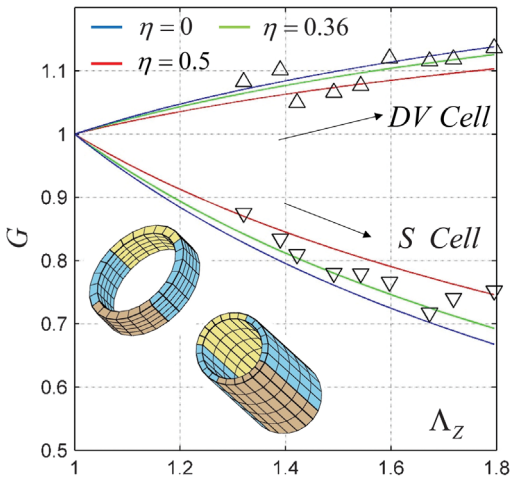

FIG. 2. Angular stretch for S and DV cells. Notice that $G_S < 1$ for S and $G_{DV} > 1$ for D cells. Theoretical curves, explained in the Supplemental Material [30], are weakly dependent of the epidermis thickness, represented by $\eta = 1 - (R_i/R_e)^2$. Comparison with experimental data from Ref. [16].

TABLE I. Geometric and elastic parameters of the model in different parts of the embryo.

	C_{0S} μm	C_{0DV} μm	λ_{0Z}	λ_{0S}	λ_{0DV}	α_1	α_2
Head	14.5	33.0	1.025	1.06	1.0326	2.2	1.27
Body	10.1	24.8	1.025	1.09	1.05	1.15	3.2
Tail	10.1	24.8	1.055	1.05	1.0232	1.25	2.9

Elastic coefficients: $\mu_{DV} = 1.44$, $\tau_S = 0.15$, $\tau_{DV} = 0.67$

The circumference lengths C_0 are extrapolated from Refs. [16,30]. λ_0, values at enclosure, differ in S and DV and from head to tail. The coefficients α's refer to active stress evolution, see Fig. 3(c). The elastic parameters of Eq. (4) do not vary along the embryo.

which fixes the ratio of stiffnesses between the S and DV cells with $\lambda_{0DV} < \lambda_{0S}$. Post enclosure, the prestrains modify the elastic strains into $\lambda = \lambda_0\Lambda = \lambda_0 Gr/R$ and $\lambda_Z = \lambda_{0Z}\Lambda_Z$ (see the Supplemental Material [30]). This explains why a tissue remains in tension even if contractile motors exert a compressive work on it. For a thin epithelium, the elastic stretch λ is transformed into $\lambda \sim \lambda_0 G/\sqrt{\Lambda_Z}$ and we have now $\sigma^p_{\theta,S} + \zeta = \sigma^p_{\theta,DV}$, which gives ζ. G_S decreases as Λ_Z increases leading to a decrease of the passive stress σ^p_θ. However, the active stress ζ, an increasing function of Λ_Z, compensates the opening of cracks in the DV direction. Finally, because the epithelial elasticity is both orthotropic and nonlinear, the adapted mathematical formula for the shape factor $\mathcal{F}_{ik}$ is deduced from W_P, Eq. (4). The equivalent Young modulus in the ith direction reads

$$E_i = K_{ii} - \frac{K_{ij}^2}{K_{jj}}; \qquad K_{ij} = \lambda_j \frac{\partial \sigma_i^p}{\partial \lambda_j} \quad \text{and} \quad \mathcal{F} \sim 2\frac{\sigma_i^p + \zeta_i}{E_i}. \tag{5}$$

This evaluation presents no difficulty once the elastic energy density is known, albeit this question remains challenging for small organisms.

Results and discussion.—The incompressibility hypothesis and the cylindrical shape are tested by comparing the angular stretch G with the experimental values of each domain: seam, dorsal, and ventral (see Fig. 2 and Table I). There is a slow dependence with the thickness of the epidermis which is reassuring since this thickness in the order of 2 μm is not known with precision. By extrapolation, we derive a value of each arclength at the "supposed" beginning of elongation and finally an angle of order $\beta \sim 26°$, indicating a significant prestretch at enclosure, associated with a prestress about 0.45 for σ_θ and 0.35 for σ_Z. As shown in Figs. 3(b) and 3(c) the amplitude of the active stress ζ is an increasing function of Λ_Z which saturates around the value 1.8. Above this value, a new mechanism involving muscle cells [39–41] occurs, not considered here as we focus on the role of the actomyosin network. Once the elastic energy W_P is obtained from the body results, this energy function is fixed everywhere: in the head and in the tail, only the prestretch values due to enclosure are very slightly modified as shown in Table I. After, the theoretical curves are derived from $\mathcal{F}$, Eq. (5) and shown in Fig. 3(a). Notice that the active stress ζ is derived from the difference between passive parts of the S and DV cells with an empirical formula of 2 parameters: $\zeta = 2\alpha_1\pi^{-1}\tan^{-1}\alpha_2(\Lambda_Z - 1)$. The agreement is good for the crack opening in S cells. All the results concerning this elongation step in the *C. elegans* embryonic life are gathered in Table I. The methodology to derive these parameters, which rest on the border conditions and available experimental data, is explained in detail in the Supplemental Material [30].

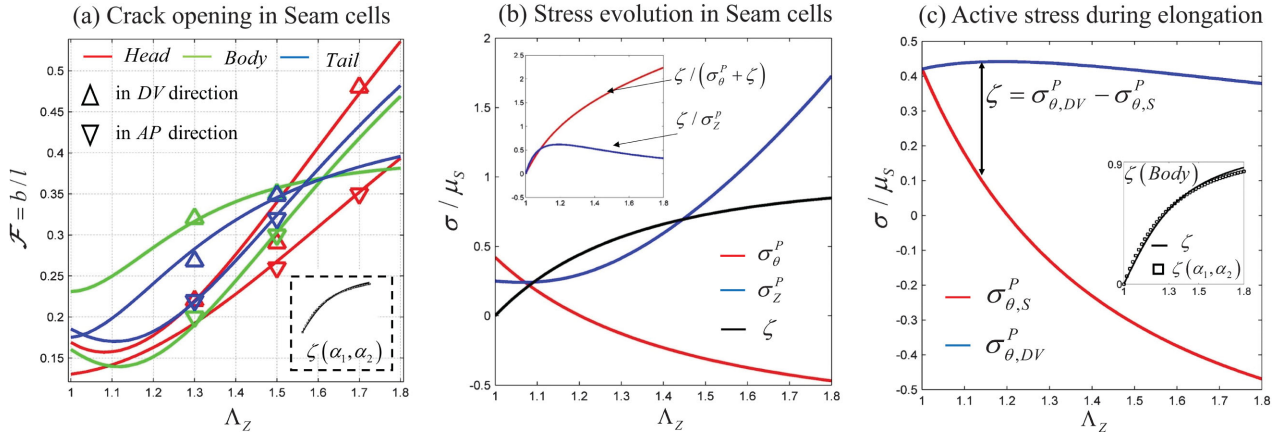

FIG. 3. (a) Crack opening in S cells for head, body and tail in the DV or AP directions, Eq. (5). Difference between curves comes from prestrain values, Table I and the Supplemental Material [30]. In the inset, the active stress ζ beginning at enclosure. (b) Comparison of passive versus active stress in S cells [Eqs. (3), (4)]. The scale for stresses is the stiffness of S cells $\mu_s = 1$. (c) Active stress evaluated as the difference of σ^p_θ between DV and S cells. In the inset, ζ, deduced from the model and approximated by $\zeta = 2\alpha_1\pi^{-1}\tan^{-1}\alpha_2(\Lambda_Z - 1)$ with 2 parameters is given in Table I.

To conclude, as emphasized in Ref. [20], it is especially delicate to extract quantitative information from nonlinear mechanical systems involving active and passive stresses and, in addition, prestretch and prestress. The complexity increases with the geometry for a multilayered inhomogeneous epidermis trapped between a central intestine and the apical ECM. *In vivo* measurements, difficult at the scale of the cell are made possible thanks to the technique of laser ablation which, combined with this analysis, gives a satisfactory picture of how molecular motors can achieve cell and embryo deformations. Even if the focus is put on *C. elegans* geometry, the theory developed here can be adapted to other systems where laser ablation is achieved to assess stresses and illustrates how prestress can be accounted for *in vivo*. The role of mechanics in embryogenesis needs not to be demonstrated anymore. However, it is crucial to develop experimental and theoretical tools to fully understand the origin of morphogenetic events in model systems.

M. B. A. would like to thank the Isaac Newton Institute of Mathematical Sciences, Cambridge, for support and hospitality during the programme "Growth, Form and Self-Organization" where work on this Letter was undertaken. M. B. A. acknowledges the partial support from the Simons Foundation, the EPSRC Grant No. EP/K032208/1 and from ANR under the Contract No. EPIMORPH (ANR-18-CE13-0008). P. Q. Q. acknowledges the support of the China Scholarship Council (CSC), file No. 201706100182. M. L. thanks the European Research Council (Grant No. 294744) for support.

*Corresponding author.
benamar@lps.ens.fr

[1] A. J. Coulombre and J. L. Coulombre, Intestinal development: I. Morphogenesis of the villi and musculature, Development **6**, 403 (1958).
[2] E. Hannezo, J. Prost, and J.-F. Joanny, Instabilities of Monolayered Epithelia: Shape and Structure of Villi and Crypts, Phys. Rev. Lett. **107**, 078104 (2011).
[3] M. Ben Amar and F. Jia, Anisotropic growth shapes intestinal tissues during embryogenesis, Proc. Natl. Acad. Sci. U.S.A. **110**, 10525 (2013).
[4] R. Toro and Y. Burnod, A morphogenetic model for the development of cortical convolutions, Cereb. Cortex **15**, 1900 (2005).
[5] A. Goriely, M. G. Geers, G. A. Holzapfel, J. Jayamohan, A. Jérusalem, S. Sivaloganathan, W. Squier, J. A. van Dommelen, S. Waters, and E. Kuhl, Mechanics of the brain: Perspectives, challenges, and opportunities, Biomech. Model. Mechanobiol. **14**, 931 (2015).
[6] M. Ben Amar and A. Bordner, Mimicking cortex convolutions through the wrinkling of growing soft bilayers, J. Elast. **129**, 213 (2017).
[7] M. Kücken and A. C. Newell, Fingerprint formation, J. Theor. Biol. **235**, 71 (2005).
[8] P. Ciarletta and M. Ben Amar, Papillary networks in the dermal–epidermal junction of skin: A biomechanical model, Mech. Res. Commun. **42**, 68 (2012).
[9] I. Heemskerk, T. Lecuit, and L. LeGoff, Dynamic clonal analysis based on chronic *in vivo* imaging allows multiscale quantification of growth in the Drosophila wing disc, Development **141**, 2339 (2014).
[10] A. D. Chisholm and J. Hardin, Epidermal morphogenesis, in *WormBook: The Online Review of C. elegans Biology* (2005).
[11] P. Nardinocchi and L. Teresi, On the active response of soft living tissues, J. Elast. **88**, 27 (2007).
[12] F. Jülicher, K. Kruse, J. Prost, and J.-F. Joanny, Active behavior of the cytoskeleton, Phys. Rep. **449**, 3 (2007).
[13] M. C. Marchetti, J.-F. Joanny, S. Ramaswamy, T. B. Liverpool, J. Prost, M. Rao, and R. A. Simha, Hydrodynamics of soft active matter, Rev. Mod. Phys. **85**, 1143 (2013).
[14] J. Prost, F. Jülicher, and J.-F. Joanny, Active gel physics, Nat. Phys. **11**, 111 (2015).
[15] S. Redemann, J. Baumgart, N. Lindow, M. Shelley, E. Nazockdast, A. Kratz, S. Prohaska, J. Brugués, S. Fürthauer, and T. Müller-Reichert, C. elegans chromosomes connect to centrosomes by anchoring into the spindle network, Nat. Commun. **8**, 15288 (2017).
[16] T. T. K. Vuong-Brender, M. Ben Amar, J. Pontabry, and M. Labouesse, The interplay of stiffness and force anisotropies drives embryo elongation, eLife **6**, e23866 (2017).
[17] A. Goriely, Five ways to model active processes in elastic solids: Active forces, active stresses, active strains, active fibers, and active metrics, Mech. Res. Commun. **93**, 75 (2018).
[18] F. Jülicher, S. W. Grill, and G. Salbreux, Hydrodynamic theory of active matter, Rep. Prog. Phys. **81**, 076601 (2018).
[19] E. Fischer-Friedrich, Y. Toyoda, C. J. Cattin, D. J. Müller, A. A. Hyman, and F. Jülicher, Rheology of the active cell cortex in mitosis, Biophys. J. **111**, 589 (2016).
[20] E. Fischer-Friedrich, Active prestress leads to an apparent stiffening of cells through geometrical effects, Biophys. J. **114**, 419 (2018).
[21] P. Theocaris, D. Pazis, and B. Konstantellos, The exact shape of a deformed internal slant crack under biaxial loading, Int. J. Fract. **30**, 135 (1986).
[22] A. Lucantonio, G. Noselli, X. Trepat, A. DeSimone, and M. Arroyo, Hydraulic Fracture and Toughening of a Brittle Layer Bonded to a Hydrogel, Phys. Rev. Lett. **115**, 188105 (2015).
[23] C. Gally, F. Wissler, H. Zahreddine, S. Quintin, F. Landmann, and M. Labouesse, Myosin II regulation during C. elegans embryonic elongation: LET-502/ROCK, MRCK-1 and PAK-1, three kinases with different roles, Development **136**, 3109 (2009).
[24] N. Fotopoulos, D. Wernike, Y. Chen, N. Makil, A. Marte, and A. Piekny, Caenorhabditis elegans anillin (ani-1) regulates neuroblast cytokinesis and epidermal morphogenesis during embryonic development, Dev. Biol. **383**, 61 (2013).
[25] S. Quintin, S. Wang, J. Pontabry, A. Bender, F. Robin, V. Hyenne, F. Landmann, C. Gally, K. Oegema, and M. Labouesse, Non-centrosomal epidermal microtubules act in parallel to LET-502/ROCK to promote C. elegans elongation, Development **143**, 160 (2016).

[26] T. T. K. Vuong-Brender, S. K. Suman, and M. Labouesse, The apical ECM preserves embryonic integrity and distributes mechanical stress during morphogenesis, Development **144**, 4336 (2017).
[27] Z. Suo, Singularities, interfaces and cracks in dissimilar anisotropic media, Proc. R. Soc. A **427**, 331 (1990).
[28] M. Ben Amar, Creases and cracks in finite elasticity, Mech. Res. Commun. **93**, 23 (2018).
[29] P. Ciarletta, M. Ben Amar, and M. Labouesse, Continuum model of epithelial morphogenesis during Caenorhabditis elegans embryonic elongation, Phil. Trans. R. Soc. A **367**, 3379 (2009).
[30] See Supplemental Material at http://link.aps.org/supplemental/10.1103/PhysRevLett.121.268102 for full description of the geometry, elasticity, fracture modeling and data analysis.
[31] A.-C. Reymann, F. Staniscia, A. Erzberger, G. Salbreux, and S. W. Grill, Cortical flow aligns actin filaments to form a furrow, eLife **5**, e17807 (2016).
[32] A. Saha, M. Nishikawa, M. Behrndt, C.-P. Heisenberg, F. Jülicher, and S. W. Grill, Determining physical properties of the cell cortex, Biophys. J. **110**, 1421 (2016).
[33] I. Bonnet, P. Marcq, F. Bosveld, L. Fetler, Y. Bellache, and F. Graner, Mechanical state, material properties and continuous description of an epithelial tissue, J. R. Soc. Interface **9**, 2614 (2012).
[34] S. Tlili, E. Gauquelin, B. Li, O. Cardoso, B. Ladoux, H. Delano-Ayari, and F. Graner, Collective cell migration without proliferation: Density determines cell velocity and wave velocity R. Soc. Open Sci., **5**, 172421 (2018).
[35] L. D. Landau and E. M. Lifshitz, *Theory of Elasticity* (Elsevier, New York, 1986), Vol. 7.
[36] R. W. Ogden, *Non-Linear Elastic Deformations* (Dover Publications, Mineola, 1997).
[37] T. C. Gasser, R. W. Ogden, and G. A. Holzapfel, Hyperelastic modelling of arterial layers with distributed collagen fibre orientations, J. R. Soc. Interface **3**, 15 (2006).
[38] G. A. Holzapfel, J. A. Niestrawska, R. W. Ogden, A. J. Reinisch, and A. J. Schriefl, Modelling non-symmetric collagen fibre dispersion in arterial walls, J. R. Soc. Interface **12**, 20150188 (2015).
[39] B. D. Williams and R. H. Waterston, Genes critical for muscle development and function in Caenorhabditis elegans identified through lethal mutations, J. Cell Biol. **124**, 475 (1994).
[40] H. Zhang, F. Landmann, H. Zahreddine, D. Rodriguez, M. Koch, and M. Labouesse, A tension-induced mechanotransduction pathway promotes epithelial morphogenesis, Nature (London) **471**, 99 (2011).
[41] R. De Vita, R. Grange, P. Nardinocchi, and L. Teresi, Mathematical model for isometric and isotonic muscle contractions, J. Theor. Biol. **425**, 1 (2017).